Pharmaceutical Sciences, 2021, 27(1), 67-75
doi:10.34172/PS.2020.63
https://ps.tbzmed.ac.ir/

Research Article

An Epithelial Sodium Channel (ENaC)-Specific Aptamer Determined through Structure-Based Virtual Screening for the Development of Hypertension Early Detection System

Dina Ratna Komala[1*], Ari Hardianto[1], Shabarni Gaffar[1], Yeni Wahyuni Hartati[1]

[1] *Department of Chemistry, Faculty of Mathematics and Natural Sciences, Universitas Padjadjaran, Indonesia.*

Article Info

Article History:
Received: 17 April 2020
Accepted: 4 August 2020
ePublished: 2 October 2020

Keywords:
-Aptamer
-Epithelial sodium channel
-Hypertension early detection system
-Molecular docking
-Molecular dynamic simulation
-Virtual screening

Abstract

Background: Epithelial sodium channel (ENaC) is a transmembrane protein involved in maintaining sodium levels in blood plasma. It is also a potential biomarker for the early detection of hypertension since the amount of ENaC is related to the familial history of hypertension. ENaC can be detected by an aptamer, a single-stranded DNA (ssDNA) or RNA which offers advantages over an antibody. This study aimed to obtain an ssDNA aptamer specific to ENaC through virtual screening.

Methods: Forty-one aptamers were retrieved from the Protein Data Bank (PDB) and the RNA was converted to ssDNA aptamers. The X-ray crystallographic structure of ENaC protein was remodelled using Modeller 9.20 to resolve missing residues. Molecular docking of aptamers against ENaC was performed using Patchdock and Firedock, then the selected aptamer was subjected to molecular docking against other ion channel proteins to assess its selectivity to ENaC. A molecular dynamics (MD) simulation was also conducted using Amber16 to acquire an in-depth understanding of the interaction within the aptamer-ENaC complex.

Results: The virtual screening suggested that the ssDNA of iSpinach aptamer (PDB: 5OB3) displayed the strongest binding to ENaC (-49.46 kcal/mol) and was selective for ENaC over the other ion protein channels. An MMGBSA calculation on the complex of aptamer-ENaC revealed binding energy of -42,12 kcal/mol.

Conclusion: The iSpinach-based aptamer is a potential probe for detecting ENaC or iDE and may be useful for the development of hypertension early detection systems.

Introduction

Hypertension or high blood pressure is a major health problem affecting about 25% of the global population. It can lead to severe health complications and increases the risk of heart disease, stroke, and even death.[1-2] Hypertension is associated with sodium salt intake which increases plasma volume, heart rate, and blood pressure. Furthermore, increased sodium levels in the blood are related to the ENaC (Epithelial Sodium Channel) protein.[3]

ENaC is a transmembrane protein that regulates sodium exchange in several tissues including the lungs, intestines, and kidneys. It is mainly involved in the reabsorption of sodium ions in the ducts of the colligentes from renal nephrons and plays a vital role in maintaining plasma sodium levels.[4] Several studies showed that ENaC consists of three main subunits, α, β and γ encoded by three genes: *SCNN1A*, *SCNN1B* and *SCNN1G*.[5-7]

ENaC is a potential biomarker for early diagnosis of hypertension and an enzyme-linked immunosorbent assay (ELISA) was developed to detect ENaC[3] revealing that the amount of ENaC is related to the familial history of hypertension. However, the ELISA method is complex and time-consuming, requiring trained personnel and expensive reagents.[8-9] Furthermore, the use of ENaC-specific antibodies in ELISA has several disadvantages, as the production of antibodies is laborious and costly due to their large molecular size. Additionally, the antibody can be affected by pH and temperature changes, with high immunogenicity and low bioavailability.[10-11]

Aptamers, single-chain oligonucleotides of DNA or RNA, offer some advantages over antibodies. They are more selective than antibodies but are relatively smaller,[12-14] and are usually selected through an *in vitro* method known as Systematic Evolution of Ligand by Exponential enrichment (SELEX). Conceptually, SELEX is simple but time-consuming and requires large resources. Moreover, it does not always produce aptamers with the desired characteristics.[15] Alternatively, an aptamer can be obtained through *in silico* methods, such as aptamer library pattern,

*Corresponding Author: Dina Ratna Komala, E-mail: dina15004@mail.unpad.ac.id

molecular docking, molecular dynamics simulation, and identification of aptamer from virtual High-Throughput Sequencing (HTS) data to identify the optimal sequence.[16] Thus, this study aimed to obtain an ENaC-specific aptamer through *in silico* approach, *i.e.* virtual screening. Initially, aptamer structures were collected from the Protein Data Bank (PDB), the RNA aptamers were converted into DNA aptamers before virtual screening against ENaC through molecular docking. Potential aptamers were then subjected to molecular docking against other proteins such as creatinine, epithelial calcium, potassium, and chloride ion protein channels. Subsequently, the molecular dynamics simulation of the selected aptamer was conducted for a more detailed analysis. Finally, a promising candidate for an ENaC-specific aptamer was identified, namely modified iSpinach aptamer, which is originally a fluorogenic RNA aptamer with a length of 69 nt.[17] This candidate can be applied in the biosensor field, specifically as a hypertensive biomarker, hence, may be important for the development of hypertension early detection systems.

Materials and Methods

Materials

The software used in this study were Amber16,[18] Biovia Discovery Studio (BDS) Visualiser,[19] Patchdock (https://bioinfo3d.cs.tau.ac.il/PatchDock/), MODELLER 9.20 (http://www.salilab.org), Mfold (http://mfold.rna.albany.edu/?=mfold), Procheck (http://www.ebi.ac.uk/), SimRNA (https://genesilico.pl/SimRNAweb/), and Visual Molecular Dynamics (VMD).[20]

The 3D structures of the ENaC (6BQN), aptamers, and other ion channel proteins were collected from the PDB (www.rcsb.org/). The protein structures retrieved from PDB were epithelial calcium channel TRPV5 (5OEO), epithelial potassium channel KCNQ1 (6UZZ), intracellular chloride ion channel CLIC1 (1K0O), and creatinine (1Q3K). The aptamers consisted of 41 structures with PDB IDs: 5OB3, 5VOE, 1EXD, 3FU2, 1HOQ, aptamer H2, 2M8Y, HS1, 1DDY, 2ARG, 2AU4, 2JLT, 4RZD, 5HRT, 2M53, 3ZH2, 1NTA, 1U1Y, 1XWP, 1Y8D, 2B63, 2L1V, 2LUN, 2QBZ, 2YIF, 3AGV, 3AHU, 3EGZ, 3IVN, 3Q3Z, 4ERJ, 4FRN, 4FRN, 4M4O, 4OQU, 4PDB, 4Q9Q, 5DO4, 5XN0, 6CK4, 6EO6, 6EVV.

Remodelling of ENaC protein

The 3D structure of ENaC (6BQN) was remodelled to resolve the missing residues via the Modeller 9.20 programme. The model with the lowest Discrete Optimised Protein Energy (DOPE) score, which was a nearer native-like,[21] was selected for further structure assessment using PROCHECK, a programme which assesses the phi and psi angular values of the ENaC amino acid residues through a Ramachandran plot.

Virtual screening of the anti-ENaC aptamer

The conversion of RNA to ssDNA aptamers was performed using BDS Visualiser. This virtual screening process utilised a Patchdock web server which employs an algorithm based on shape complementarity principles. The ENaC structure, consisting of α, β and γ subunits, functions as the receptor, whereas each aptamer structure was the ligand. Clustering Root-Mean-Square Deviation (RMSD) was 4 Å, with default complex type. The docking results were further refined by Firedock, with the aptamer selected according to the binding energy of each complex which was represented by the atomic contact energy.

Selectivity assessment of the aptamer to ENaC

The selected aptamer from virtual screening was subjected to molecular docking against other ion channel proteins including TRPV5, KCNQ1, CLIC1, and creatinine. The resulting docking solutions were refined using Firedock, with the selectivity determined by the Firedock binding energy scoring of each complex.

Molecular dynamics (MD) simulation preparation and protocol

The MD simulation system was prepared with the *tleap* programme in AmberTools16. The aptamer-ENaC complex was solvated with explicit water molecules (TIP3P), the minimum distance between the protein and box boundary was 10Å, with Na^+ and Cl^- ions added to the system to achieve neutral charges.

The MD simulation was performed using a GPU-accelerated Particle Mesh Ewald Molecular Dynamics (PMEMD) in Amber16.[18] Two steps of energy minimisation were conducted with restraining protein-aptamer complex by 25 and 5 $kcal^{-1}$. $Å^{-2}$. The system temperature was raised to 300 K under NVT conditions, followed by equilibration steps for 50 ps. The system density was equilibrated to 1 $g.cm^{-1}$ for the next 50 ps NPT simulation. In the subsequent NVT simulation, the restraint on the protein-aptamer complex was removed every 50 ps, then eliminated in the last equilibrium step of 50 ps.

The production-phase was simulated under the NPT at 300 K and employed a Particle Mesh Ewald (PME)[22] method for long-range electrostatic interactions and a 10 Å cut-off for short-range non-bonded interactions.[23-24] A SHAKE algorithm was used to constrain all bonds involving hydrogen atoms.[25] The production step was conducted to yield a 100-ns MD trajectory.

Binding energy calculation

The binding energy values of aptamer and ENaC protein were calculated using the MMGBSA (Molecular Mechanics Generalised Born Surface Area) method[26] implemented in MMPBSA.py[27] to determine the estimated binding energy values of the aptamer to ENaC protein as well as their per-residue decomposition. MMGBSA does not incorporate conformational entropy or the free energy of water molecules in the binding site, although these components may have a role in protein-ligand interactions. Nevertheless, the MMGBSA method has been applied successfully to rational experimental data and

to improve the results of virtual screening and docking.[28] The MMGBSA binding free energy (ΔG° MMGBSA) was calculated as follows in Eq. 1.

$$\Delta G^{\circ}_{MMGBSA} = Gcom_i - \langle Grec \rangle_i - \langle Glig \rangle_i \quad \text{Eq. (1)}$$

Where $\langle G_{com} \rangle_i$, $\langle G_{rec} \rangle_i$, and $\langle G_{lig} \rangle_i$ are the average value of $\Delta G^{\circ}_{MMGBSA}$ for complex, ENaC and aptamer, i extracted from MD trajectories. G_x can be decomposed as shown in the Eq. 2:

$$G_x = E_{MM} + G^{GB}_{Solv} + G^{SA}_{Solv} \quad \text{Eq. (2)}$$

Where E_{MM} is the gas phase energy, G^{GB}_{solv} is the electrostatic portion of solvation energy computed using Generalised Born (GB) implicit solvent model, and G^{SA}_{solv} is the hydrophobic contribution to the solvation energy. Molecular mechanics energy consists of the bond (E_{bond}), angle (E_{angle}), torsion energies ($E_{torsion}$), van der Waals (E_{vdW}), and electrostatic interactions (E_{el}) (Eq. 3).

$$E_{MM} = \Sigma_{bonds} E_{bond} + \Sigma_{angles} E_{angle} + \Sigma_{torsions} E_{torsion} + E_{vdW} + E_{electrostatic} \quad \text{Eq. (3)}$$

Visualisation and MD trajectory analysis

Structure visualisation, MSEP generation, and non-bonded interactions were conducted using BDS Visualiser. The cpptraj programme in AmberTools16[18] was utilised to analyse MD trajectories. The analysis consisted of hydrogen bond conservation, Root-Mean-Square Fluctuation (RMSF) and RMSD. The extraction of the last frame of the MD trajectory was performed using VMD.

Results and Discussion

Remodelling of ENaC protein

The crystal structure of the ENaC protein is available in the PDB consisting of a homotrimer with three subunits: *α*, *β*, and *γ* (with PDB ID: 6BQN).[29] However, the structure has a considerable number of missing residues as depicted in the PDB web server (https://www.rcsb.org/pdb/explore/remediatedSequence.do?structureId=6BQN) (Figure S1), which may mislead the results, so the ENaC protein was remodelled using Modeller 9.20 software.[30]

The remodelling of the ENaC protein was conducted using 6BQN as a template, producing 50 structural models. One criterion for selecting the best model is the DOPE value, which indicates the potential energy of the model. The best model was judged according to the lowest DOPE value since it represents a nearer native-like.[21] In our study, the best model had a DOPE of -148683.03 (Figure S2). Furthermore, the model was assessed using the Ramachandran plot to evaluate the percentage of amino acids in the allowed regions, which is an important indicator of the quality of the structural model.

Evaluation of the ENaC model

The ENaC model was evaluated using the PROCHECK programme. The Ramachandran plot illustrates the possibility of secondary structure types based on phi and psi angles, with the quality of the 3D structure determined by inspecting the angles of non-glycine residues located in dis-allowed regions.[31] According to the Ramachandran plot, the criterion for a good model is at least 90% of non-glycine residues having phi and psi angles in the allowed regions. Our results show that the best model fulfils the criterion, with the phi and psi angles of 90.9% of non-glycine residues in the allowed regions. Moreover, only three residues of the best model possess phi and psi angles in the dis-allowed region, D102 of the alpha subunit and A970 and E996 of the gamma subunit which are located in the loop regions.

To improve the model quality, the loop region was further optimised utilising Modeller 9.20 around the residues with phi and psi angles in the dis-allowed regions. The optimised model (Figure S3) was evaluated using PROCHECK, revealing that the number of residues having phi and psi angles in the allowed regions increased to 91.1%, while those in the dis-allowed region disappeared (Figure S4).

Virtual screening of aptamers from PDB against ENaC

Forty-one aptamers were retrieved from PDB and the RNA aptamers were converted to ssDNA using BDS. By employing Patchdock and Firedock web servers, each aptamer was subjected to molecular docking with ENaC as the target receptor. The molecular docking procedure was the screening step to obtain the aptamer with the strongest binding affinity to ENaC. The results of molecular docking including docking scores and predicted binding energy values are tabulated in Table 1.

Initially, virtual screening was performed on the Patchdock web server which implements three major stages of shape complementarity principles: molecular shape representation, surface patch matching, as well as filtering and scoring.[32] In the first stage, the molecular surfaces of the aptamers and ENaC were computed. Geometric patches on aptamers and ENaC, which can be flat, convex, and concave surfaces, were detected using a segmentation algorithm and filtered to retain only important residues, which were then matched by utilising a matching technique combination of Pose-Clustering and Geometric Hashing. All complexes with steric collisions between the atoms of ENaC and aptamers were eliminated, while the remaining complexes were ranked based on a geometric shape complementarity score. According to the Patchdock results, the aptamer with PDB ID 3Q3Z had the highest score, however, Patchdock is a rigid-body docking algorithm, so the resulting docking solutions of each aptamer-ENaC complex were further refined using Firedock.

Firedock refined docking solutions of each aptamer-ENaC complex using restricted interface side-chain rearrangement and soft rigid-body optimisation. The flexibility of sidechains was modelled by rotamers, whereas their rearrangements were solved by integer linear programming.[33] In the following step, Monte Carlo

Table 1. Docking and binding energy scores between each aptamer and ENaC. Docking scores, which are geometric shape complementarity scores, were obtained from Patchdock, whereas binding energy scores were generated by Firedock.

No.	Aptamer	Docking score	Binding Energy (Kcal/mol)
1	5OB3	22354	-49.46
2	1XWP	12086	-43.96
3	2JLT	16206	-40.61
4	3IVN	23880	-39.77
5	HS1	13862	-37.94
6	6EO6	12776	-36.95
7	4M4O	16418	-35.71
8	4PDB	16522	-33.73
9	2YIF	20932	-32.56
10	1NTA	17160	-32.20
11	H2	17974	-32.09
12	1EXD	21890	-32.04
13	5VOE	17344	-31.91
14	1HOQ	11240	-28.43
15	6CK4	20494	-27.68
16	2M53	14956	-26.59
17	2LUN	16056	-26.39
18	4FRN	21128	-25.33
19	2L1V	15126	-24.60
20	3AHU	11058	-24.31
21	3FU2	20634	-23.80
22	4RZD	22260	-23.76
23	3Q3Z	25860	-23.26
24	6EVV	14104	-22.93
25	2QBZ	19542	-21.08
26	2m8y	12740	-21.06
27	4Q9Q	21744	-20.74
28	4ERJ	22154	-20.70
29	2ARG	14698	-20.60
30	3EGZ	19958	-20.29
31	5HRT	15774	-19.12
32	2AU4	17556	-18.93
33	5DO4	16906	-18.68
34	4OQU	19364	-18.07
35	1U1Y	13066	-18.02
36	3AGV	15756	-17.78
37	1Y8D	15690	-13.53
38	5XN0	18148	-11.85
39	1DDY	18398	-11.71
40	3ZH2	16392	-11.70
41	2B63	19548	-11.42

minimisation of the binding score function refined the relative position of the aptamer and ENaC. The ranking of the refined docking solutions was based on a binding score which consists of partial electrostatics, softened van der Waals interactions, atomic contact energy,[34] and additional approximations of the binding free energy. The refinement results are summarised in Table 1, which tabulates the binding energy scores of the best docking solutions for each aptamer and ENaC complex.

The refined docking solutions (Table 1) suggested that the DNA aptamer adapted from 5OB3 forms the strongest binding to ENaC. This aptamer, hereafter is called iSpinach-based aptamer for detecting ENaC (iDE), showed the most negative binding score of -49.46 kcal/mol. It is an ssDNA version of iSpinach aptamer, which is a fluorogenic RNA aptamer interacting specifically with small molecules and increasing fluorescence in the formation of complex compounds.[17] It is a potential aptamer for the development of hypertension early detection systems, thus, needs further evaluation of its selectivity to ENaC.

Assessing the selectivity of iDE to ENaC

To assess its selectivity to ENaC, iDE was subjected to other molecular docking procedures against epithelial calcium, potassium, and chloride ion channels as well as creatinine. This step also employed Patchdock to generate initial docking solutions of each iDE-protein complex and Firedock for refinement and reranking purpose (Table 2).

Table 2 suggests that the interaction between iDE and ENaC is the strongest, with a binding energy of -49.46 kcal/mol. Interestingly, the binding of iDE to other protein ion channels is weaker than that to ENaC, implying the selectivity of the aptamer to ENaC. Meanwhile, the complex of iDE and creatinine has a binding energy of -43.64 kcal/mol, which is 5.82 kcal/mol weaker than iDE and ENaC binding energy. Nevertheless, 5.82 kcal/mol is not a large difference in binding energy. Thus, the measurement of ENaC using iDE as the biosensor probe could be interfered by the presence of creatinine in the urine. Fortunately, data treatment of the response pattern using chemometrics may alleviate such an issue.[35]

The docking of iDE to ENaC and creatinine (Figure 1) revealed that the aptamer binds to both proteins in a shape complementarity fashion. Nonetheless, both iDE-ENaC (Figure 1a and b) and -creatinine complexes (Figure 1c and d) portray negative charges at the binding patch, which may cause repulsive interaction with the negatively charged iDE (Figure 1a and c). As shown in Table S1, the iDE-ENaC complex shows only one unfavourable interaction of negative-negative charge between Asp393 and nucleotide C67 (Figure 2), whereas the iDE-creatinine complex possesses two repulsive interactions.

Although a visual inspection (Figure 1) may suggest the portion of iDE molecule binding to ENaC is higher than

Table 2. Binding energy (kcal/mol) comparison of iDE against ENaC and other ion channel proteins.

No	Protein	PDB ID	Binding energy
1	ENaC	6BQN	-49.46
2	Epithelial calcium channel	5OEO	-24.94
3	Epithelial potassium channel	4V0C	-22.27
4	Intracellular chloride ion channel	1K0O	-27.44
5	Creatinine	1Q3K	-43.64

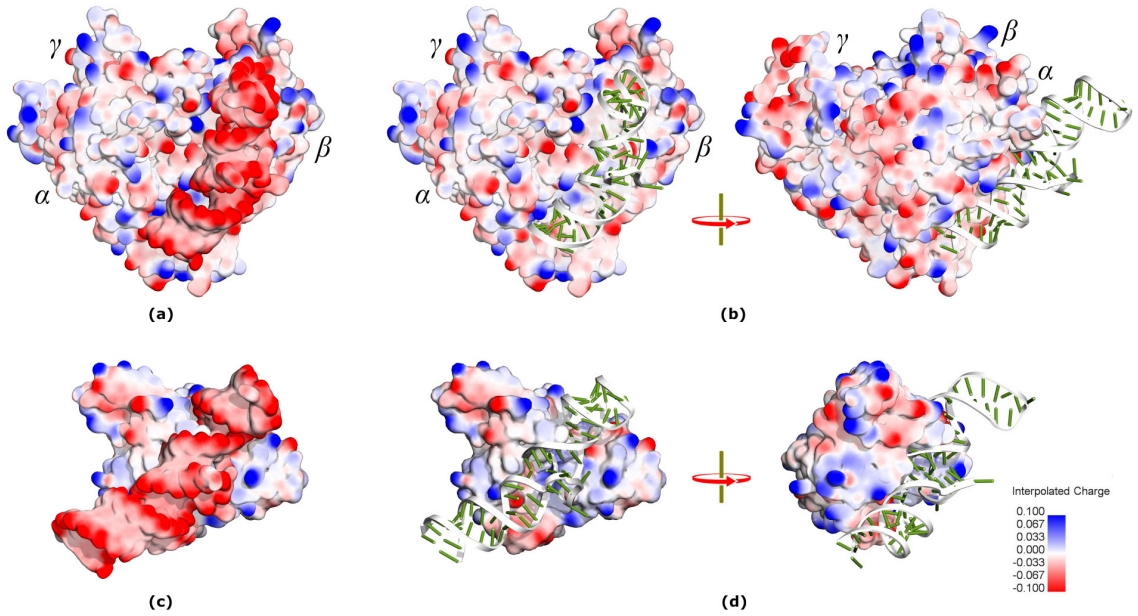

Figure 1. The docking of iDE to ENaC and creatinine resulted by Patchdock and Firedock web servers. The binding of iDE molecule to ENaC is depicted in (a) Molecular Surface Electrostatic Potential (MSEP) and (b) ladder and arrow representations. Meanwhile, (c) shows MSEPs of iDE and creatinine complex, while (d) portrays the iDE molecule in ladder and arrow representation binding to the MSEPs of creatinine.

that to creatinine, ΔSASAs of both complexes, which represent contact areas between iDE and its protein partner, showed that the iDE-creatinine complex has a higher ΔSASA (1762.85 Å) than iDE-ENaC (1414.17 Å), indicating more intense interactions created when it binds to creatinine than to ENaC.

As listed in Table S2, the binding of iDE to creatinine involves thirteen electrostatic, six hydrogen bonds, and eight hydrophobic interactions. The complex of iDE-creatinine, however, also includes sixty-four unfavourable interactions contributed by twenty-four pairs of amino acid and nucleotide base residues. Meanwhile, ENaC interacts

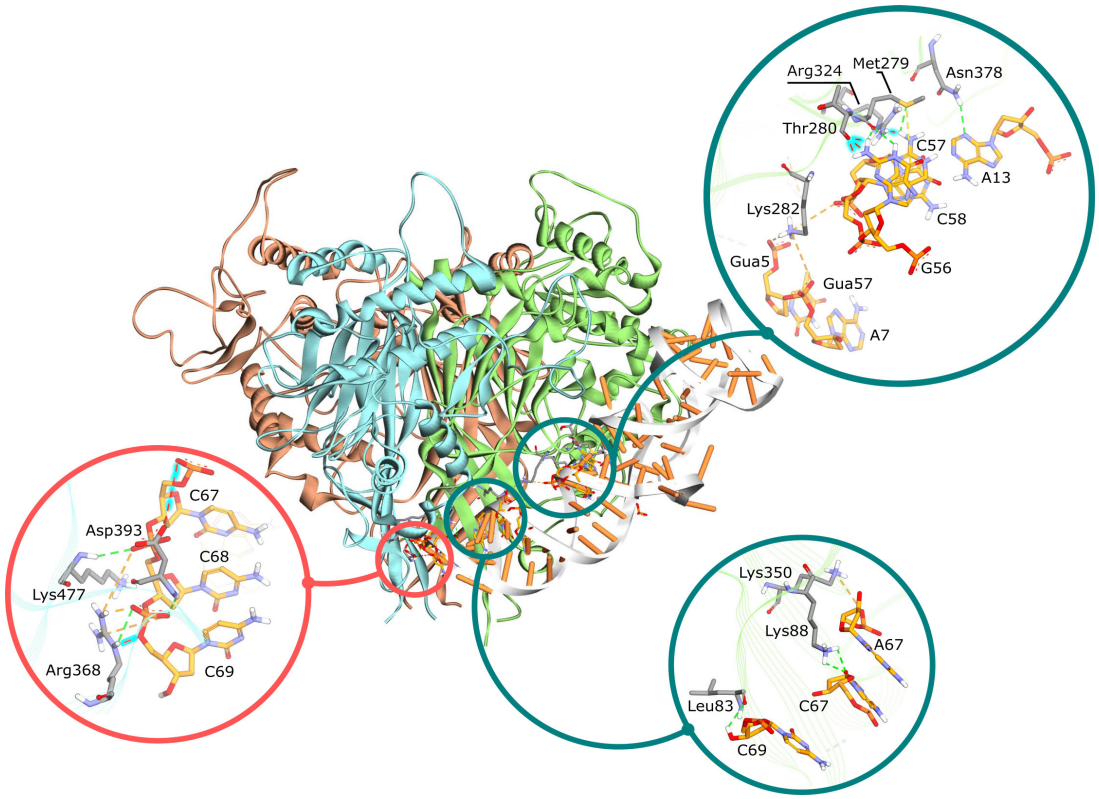

Figure 2. The molecular docking of iDE to ENaC resulted by Patchdock and Firedock web server, the binding of iDE to ENaC involves ten hydrogen bonding interaction (Asp393-C69, Lys477- C68, Arg386-C69), seven electrostatic interaction (Lys282-C58, Lys282-A7), onepi-Sulfur (Met279-G57) and six unfavourable interactions (Thr280-G56, Arg324-G57).

more frequently through its α subunit than β when it binds iDE (Table S1 and Figure 2).

The binding of iDE and ENaC undergoes via one pi-sulphur, seven electrostatic, and ten hydrogen bond interactions, with a total of six unfavourable interactions from four pairs of amino acid and nucleotide base residues (Figure 2). The low number of unfavourable interactions in the iDE-ENaC complex (Table S3) may explain its stronger binding score than iDE-creatinine complex (Table S4).

MD simulation of the iDE-ENaC complex

For a more in-depth understanding of the iDE and ENaC binding, an MD simulation was performed with a trajectory of 100 ns. From the trajectory, RMSD was used to compare the changes in the molecular conformation of iDE and ENaC during binding (Figure 3), showing that ENaC exhibits a small conformational change, starting from 30 until 100 ns, which may reflect the structural stability of the protein, whereas a large conformational change occurs in the iDE molecule. For the follow-up investigation, RMSF analysis was applied for iDE and each subunit of ENaC. In contrast to RMSD, RMSF was calculated for each residue in ENaC or iDE, describing the conformational shift of each amino acid in ENaC or nucleotide residue in iDE. The α subunit shows the most fluctuated RMSF profile (Figure 4), particularly around the residue of 169, 198, and 217, located at the loop regions where some residues interact with iDE. The great structural change of the α subunit at the loop regions are also depicted in Figure 5, while the β and γ subunits exhibit relatively small conformational shifts.

Most residues of the iDE display RMSF values above 2 Å (Figure 4d). The iDE aptamer fluctuates in several nucleotide residues, especially in the middle, with the highest within the position of 32–33 with RMSF values of 8.24–8.34 Å (Figure 5), where the iDE molecule shows a conformational change. Additionally, according to the last frame of the MD trajectory, the whole molecule of iDE shifted from the initial binding position with ENaC by molecular docking, which may reflect the altered interaction between iDE and ENaC.

The analysis of the MD trajectory last frame reveals the altered interactions between iDE and ENaC (Table S5). Some amino residues, which previously contributed to the

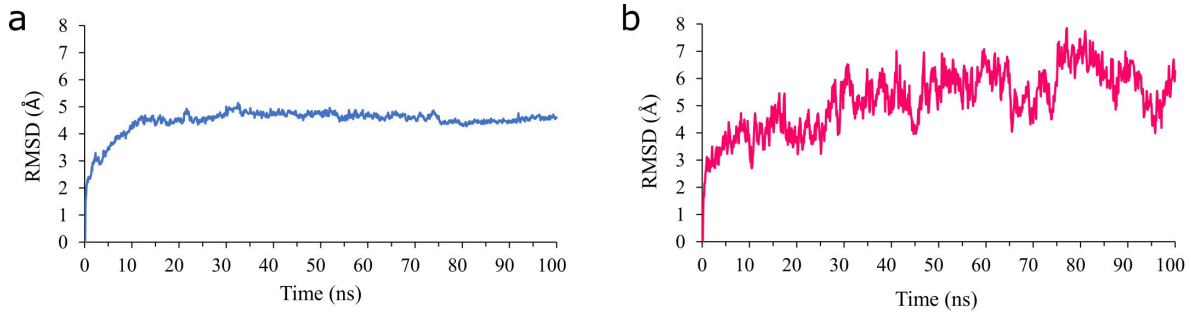

Figure 3. Root Mean Square Deviation (RMSD) profile of (a) ENaC Protein subunits α, β, γ and (b) iDE aptamer during 100 ns molecular dynamics simulation

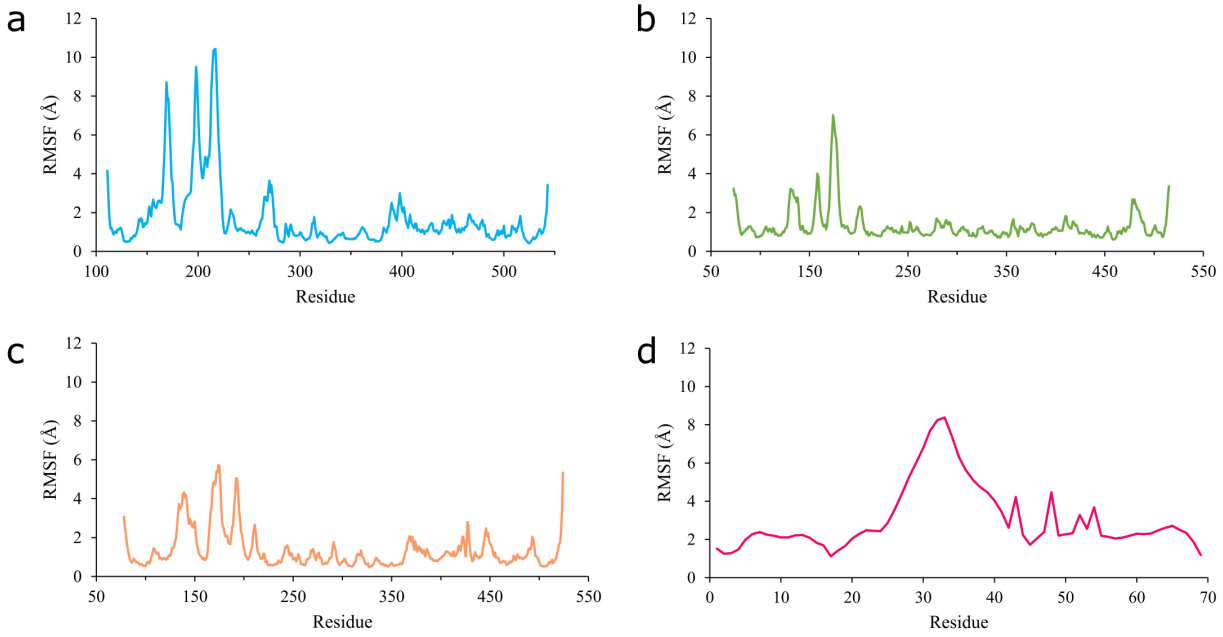

Figure 4. Root Mean Square Fluctuation (RMSF) profile of all residues ENaC subunit (a) α, (b) β, (c) γ and (d) iDE aptamer during molecular dynamics simulation.

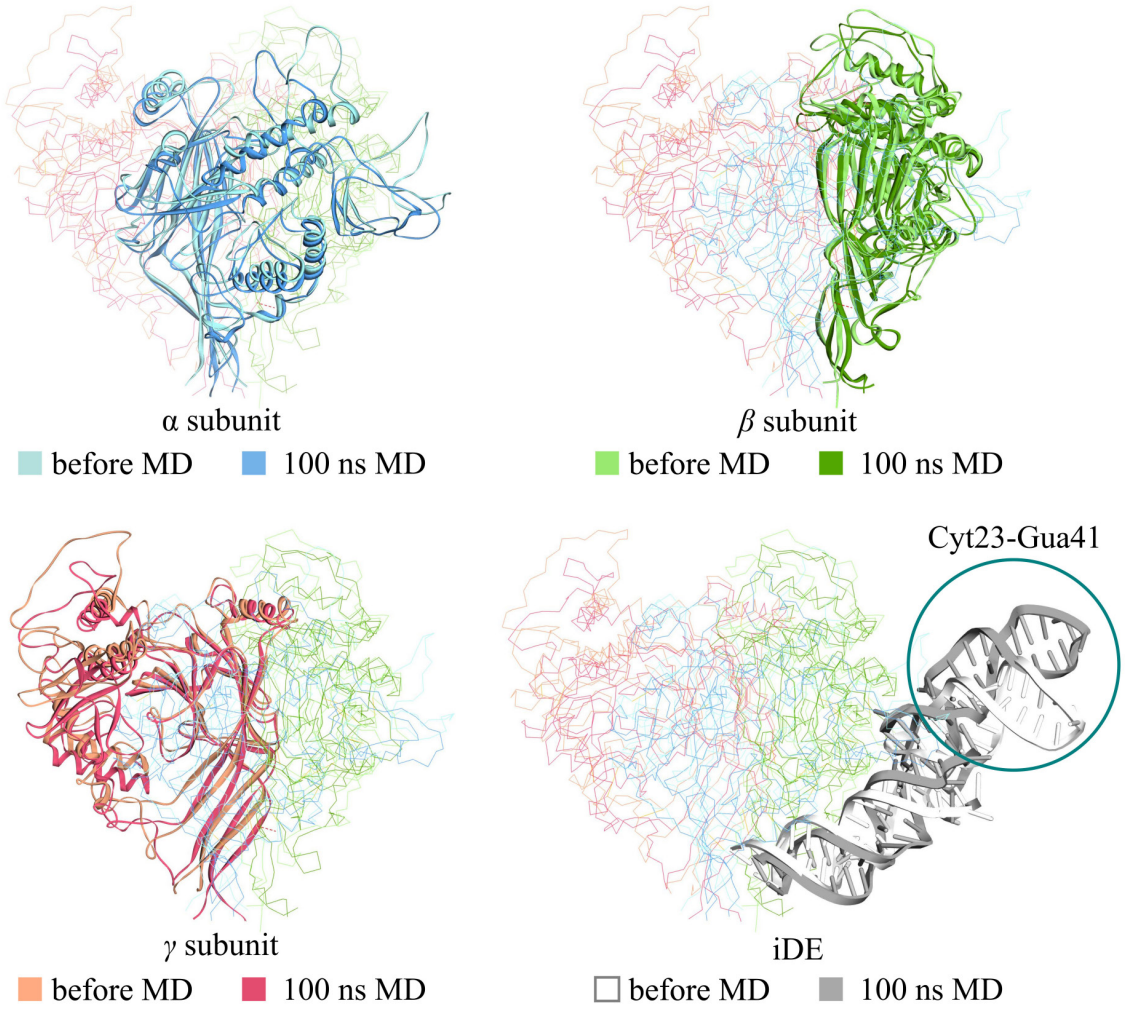

Figure 5. The molecular conformational change of ENaC subunits α, β, γ and iDE before and after 100 ns MD, during simulation ENaC exhibits a small conformational change, meanwhile iDE molecule undorgoes a large conformational change. The iDE aptamer fluctuates in several nucleotide residues, especially in the middle nucleotide (Cyt23-Gua41).

electrostatic and hydrogen bond interactions in the iDE-ENaC complex based on the best docking solution, do not participate in the binding, including Leu83, Lys88, Asn378, Arg386, and Asp393. Nonetheless, other residues (Met279, Lys282, Lys350, Lys477) of ENaC interact with iDE, with other amino acid residues of ENaC α and β subunits forming new interactions with iDE (Table S5).

Hydrogen bond conservation was also extracted from the MD trajectory of the iDE-ENaC complex (Table S6). This analysis not only included hydrogen bonds but also electrostatic interactions. Two of four residues of the ENaC β subunit, which display non-bonded interactions in both iDE-ENaC complexes from the docking solution and MD trajectory, show considerable hydrogen bond conservation, Met279 and Lys350. The carbonyl group of the Met279 backbone interacts with the primary amine hydrogen atom of G57 with the conservation of 52.2%. The Lys350 residue of the ENaC β subunit and the phosphate group of A4 form three hydrogen bonds occurring in 32.5%, 21.5%, and 20.4% in the 100-ns MD trajectory. Among other new interactions appearing in the MD simulation, the first and the second most persistent hydrogen bonds (71.8 and 56.2% occurrence) are contributed by Ser263. Overall, hydrogen bonds with conservation above 30% are contributed by amino acid residues from the ENaC β subunit, particularly Ser263, Met279, Asn260, Arg324, Ser82, Leu83, and Lys350. These residues may form the key interactions in the binding of iDE to ENaC.

The binding energy between iDE and ENaC was analysed from the 100-ns MD trajectory using the MMGBSA method.[26] Molecular mechanics energy consists of the bond (E_{bond}), angle (E_{angle}), torsion energies ($E_{torsion}$), van der Waals (E_{vdW}), and electrostatic interactions (E_{el}).[26] The calculated total energy values between ENaC and iDE are -42,12 kcal/mol.

Conclusion

In this study, forty-one aptamers from PDB were virtually screened against ENaC using molecular docking. The aptamers consisting of ssDNA and RNA ones were converted to ssDNA before virtual screening, identifying a promising aptamer ssDNA aptamer originally from a fluorogenic RNA aptamer, *iSpinach,* with PDB ID 5OB3 and a length of 69 nt. The aptamer was named iDE

(iSpinach-based aptamer for detecting ENaC) and showed the strongest (-49.46 kcal/mol) binding to ENaC according to the Firedock binding energy scoring. Moreover, molecular docking of iDE to other ion channel proteins and creatinine suggested the selectivity of the aptamer to ENaC. The binding of iDE and ENaC is based on the shape and electrostatic complementarity, as inferred by MSEP visualisation. Meanwhile, the MD simulation implied that the key amino acid residues in the binding of iDE are within the ENaC β subunit, particularly Ser263, Met279, Asn260, Arg324, Ser82, Leu83, and Lys350. In summary, iDE is a potential ENaC-specific aptamer for the development of hypertension early detection systems and binds to ENaC with an MMGBSA binding energy of -42,12 kcal/mol.

Acknowledgements

This work was supported by PTM and PDUPT scheme researches of Indonesian Ministry of Research, Technology and Higher Education No. 2776/UN6.D/LT/2019.

Conflict of Interest

The authors claim that there is no conflict of interest.

Supplementary Data

Supplementary file contains Figures S1-S4 and Tables S1-S6 is available on the journal's web site along with the published article.

References

1. Toka HR, Koshy JM, Hariri A. The molecular basis of blood pressure variation. Pediatr Nephrol. 2013;28:387-99. doi:10.1007/s00467-012-2206-9
2. Whelton PK, Carey RM, Aronow WS. ACC/ AHA/ AAPA/ABC/ACPM/AGS/APhA/ASH/ASPC/NMA/ PCNA guideline for the prevention, detection, evaluation, and management of high blood pressure in adults: A report of the american college of cardiology/ american heart association task force on cinical practice guidelines. J Am Coll Cardiol. 2017; 71(6):1269-1324. doi:10.1161/HYP.0000000000000066
3. Sofiatin Y, Roesli RMA. Detection of urinary epithelial sodium channel (ENaC) protein. Am J Clin Med Res. 2018;6(2):20-3. doi:10.12691/ajcmr-6-2-1
4. Loffing J, Schild L. Functional domains of the epithelial sodium channel. J Am Soc Nephrol. 2005;16(11):3175-81. doi:10.1681/ASN.2005050456
5. Bhalla V, Hallows KR. Mechanisms of ENaC regulation and clinical implication. J Am Soc Nephrol. 2008;19(10):1845-54. doi:10.1681/ASN.2008020225
6. Garty H, Palmer LG. Epithelial sodium channels: function, structure, and regulation. Physiol Rev. 1997;77:359-96. doi:10.1681/ASN.2008020225
7. Kashlan OB, Kleyman TR. ENaC structure and function in the wake of a resolved structure of a family member. Am J Physiol Renal Physiol. 2011;30:684-96. doi:10.1152/ajprenal.00259.2011
8. Rajesh, Singal S, Kotnala RK. Single Frequency Impedance Analysis on Reduced Graphene Oxide Screen-Printed Electrode for Biomolecular Detection. Appl Biochem Biotechnol. 2017;183:672-83. doi:10.1007/s12010-017-2510-8
9. Tuteja SK, Ormsby C, Neethirajan S. Nanoinvasive Label-Free detection of cortisol and lactate using graphene embedded screen-printed electrode. NanoMicro Lett. 2018;10(3):41. doi:10.1007/s40820-018-0193-5
10. Chen A, Yang S. Replacing antibodies with aptamers in lateral flow immunoassay. Biosens Bioelectron. 2015;71:230-42. doi:10.1016/j.bios.2015.04.041
11. Nimjee SM, White RR, Becker RC, Sullenger BA. Aptamer as therapeutics. Annu Rev Pharmacol Toxicol. 2017;57:61-79. doi:10.1146/annurev-pharmtox-010716-104558
12. Sun H, Zhu X, Lu PY, Rosato RR, Tan W, Zu Y. Oligonucleotide aptamers: new tools for targeted cancer therapy. Mol Ther Nucleic Acids. 2014;3:182. doi:10.1038/mtna.2014.32
13. Kinghorn AB, Tanner JA. Selective phenome growth adapted model: a novel landscape to represent aptamer ligand binding. complexity. 2017:6760852. doi:10.1155/2017/6760852
14. Trausch JJ, Retzlaff MS, Verch T. Replacing antibodies with modified DNA aptamers in vaccine potency assays. Vaccine. 2017;35(41):5495-502. doi:10.1016/j.vaccine.2017.04.003
15. Mckeague M, Derosa MC. Challenges and opportunities for small molecule aptamer development. J Nucleic Acids. 2012;2012:748913. doi:10.1155/2012/748913
16. Kinghorn AB, Fraser LA, Liang S, Shiu SCC, Tanner JA. Aptamer bioinformatics. Int J Mol Sci. 2017;18(12):2516. doi:10.3390/ijms18122516
17. Millan PF, Autour A, Ennifar E, Westhof E, Ryckelynck M. Crystal structure and fluorescence properties of the iSpinach aptamer in complex with DFHBI. RNA. 2017; 23:1788-95. doi:10.1261/rna.063008.117
18. Case DA, Betz RM, Botello-smith W, Cerutti DS, Cheatham TE III, Darden TA, et al. Amber 2016. University of California, San Francisco; 2016.
19. Dassault Systèmes BIOVIA. Discovery studio visualizer. San Diego; 2016.
20. Humphrey W, Dalke A, Schulten K. VMD: visual molecular dynamics. J Mol Graph. 1996;14(1):33-38. doi:10.1016/0263-7855(96)00018-5
21. Eswar N, Eramian D, Webb B, Shen MY, Sali A. Protein structure modeling with MODELLER. Methods Mol Biol. 2008;426:145-159. doi:10.1007/978-1- 60327-058-8_8
22. Darden T, York D, Pedersen L. Particle mesh Ewald: an N·log(N) method for Ewald sums in large systems. J Chem Phys. 1993;98(12):10089-92. doi:10.1063/1.464397
23. Fisette O, Wingbermuhle S, Tampe R, Schafer LV. Molecular mechanism of peptide editing in the tapasin-MHC I complex. Sci Rep. 2016;6:19085. doi:10.1038/

srep19085
24. Kumar A, Cocco E, Atzori L, Marrosu MG, Pieroni E. Structural and dynamical insights on HLA-DR2 complexes that confer susceptibility to multiple sclerosis in Sardinia: a molecular dynamics simulation study. PLoS One. 2013;8(3):e59711. doi:10.1371/journal.pone.0059711
25. Ryckaert JP, Ciccotti G, Berendsen HJC. Numerical integration of the cartesian equations of motion of a system with constraints: molecular dynamics of n-alkanes. J Comput Phys. 1977;23(3):327-41. doi:10.1016/0021-9991(77)90098-5
26. Gohlke H, Case DA. Converging free energy estimates: MM-PB(GB)SA studies on the protein–protein complex Ras–Raf. J Comput Chem. 2004;25(2):238-50. doi:10.1002/jcc.10379
27. Miller BR, McGee TD, Swails JM, Homeyer N, Gohlke H, Roitberg AE. MMPBSA.Py: an efficient program for end-state free energy calculations. J Chem Theory Comput. 2012;8(9):3314-21. doi:10.1021/ct300418h.
28. Genheden S, Ryde U. The MM/PBSA and MM/GBSA methods to estimate ligand-binding affinities. Expert Opin Drug Discov. 2015;10(5):449-61. doi:10.1517/17460441.2015.1032936
29. Noreng S, Bharadwaj A, Posert R, Yoshioka C, Baconguis I. Structure of the human epithelial sodium channel by cryo-electron microscopy. Elife. 2018;7:e39340. doi:10.7554/eLife.39340.
30. Fiser A, Sali A. Comparative Protein Structure Modelling with Modeller: A Practical Approach. http://salilab.org/modeller/methenz/andras.andras.html.
31. Holtje HD, Sippl W, Rognan D, Folkers G. Molecular Modelling, Basic Principle and Application. Weinhem: WILEY-VCH Verlag GmbH & Co. KGaA; 2008. p. 31-52.
32. Schneidman-Duhovny D, Inbar Y, Nussinov R, Wolfson HZ. Patchdock and symmdock: servers for rigid and symmetric docking. Nucleid Acid Res. 2005;33(Web Server issue):W363-7. doi:10.1093/nar/gki481
33. Kingsford CL, Chazelle B, Singh M. Solving and analyzing side-chain positioning problems using linear and integer programming. Bioinformatics. 2005;21(7):1028-36. doi:10.1093/bioinformatics/bti144
34. Zhang CG, Vasmatzis JL, Cornette, DeLisi C. Determination of atomic desolvation energies from the structures of crystallized proteins. J Mol Biol. 1997;267(3):707-26. doi:10.1006/jmbi.1996.0859.
35. Cuypers W, Lieberzeit PA. Combining Two Selection Principles: Sensor Arrays Based on Both Biomimetic Recognition and Chemometrics. Front Chem. 2018;6:268. doi:10.3389/fchem.2018.00268